Experimental and Theoretical Study on the Transformation Behavior of Bisphenol S by Radicals Driven Persulfate Oxidation

Junyan Wei
Nanjing University
Linning Yin
Nanjing University
Ruijuan Qu
Nanjing University
Gadah Al-Basher
King Saud University
Xiaoxue Pan (panxiaoxue1208@163.com)
Anhui University
Zunyao Wang
Nanjing University

Research Article

Keywords: Bisphenol S, Persulfate, Radicals, Transition State, Transformation mechanism

Posted Date: June 24th, 2021

DOI: https://doi.org/10.21203/rs.3.rs-460672/v1

Abstract

An in-depth study on the degradation of bisphenol S (BPS) by both single-walled carbon nanotubes and heat activated persulfate (PS) was investigated in detail. The factors like materials dosage, initial substrate concentration, initial pH and water matrix on removal of BPS were evaluated and 10 μM BPS could be completely removed in 90 min under the optimal conditions of $[BPS]_0$: $[PS]_0$ = 1: 100, T = 25 ℃, pH_0 = 7.0, [N-SWCNTs] = 20 mg·L^{-1}. Fast removal of BPS was also obtained when reaction temperature reached 65 ℃ without catalyst. There were 15 intermediates identified in total; and hydroxylation, sulfate addition, carboxylation, the cleavage of S − C bond and polymerization were considered as the main transformation pathways of BPS in both two systems based on LC-MS analysis. The proportion discrepancy of •OH and $SO_4^{\bullet-}$ involved in two systems led to different distribution and abundance of observed products. The results of transition state calculation further confirmed the reaction potential of hydroxylation, hydrogen atom abstraction and sulfate addition, and the minimum reaction barriers were 22.20, 25.06 and 13.85 kJ/mol, respectively. The present work firstly reveals the overall transformation behavior of BPS in radicals-triggered PS system by combining experimental and theoretical study.

1. Introduction

Bisphenol S (BPS), a substitution product of bisphenol A (BPA), is tremendously utilized as the original materials of some esters (e.g., makrolon), additives and fire retardants etc. due to the conspicuous properties. Previous studies have showed that BPS has been widely detected in food (Liao and Kannan, 2014b; Cao et al., 2019; Zhou et al., 2019), paper products (Liao et al., 2012b), personal care products (Liao and Kannan, 2014a), surface water (Yamazaki et al., 2015; Jin and Zhu, 2016; Liu et al., 2017b), indoor dust (Liao et al., 2012a; Wang et al., 2015a) and even in human urine (Liao et al., 2012a; Ye et al., 2015; Lehmler et al., 2018). Its detection frequency and concentrations are comparable with BPA. For example, Cao et al. (2019) measured BPS and BPA in food composite samples at the concentrations level of 1.2–35.0 ng/g and 5.3–41.0 ng/g, and the detection frequency was 5.9% and 6.2%, respectively. Furthermore, the BPS content increased over years (Jin and Zhu, 2016; Liu et al., 2017b). It is proven that this compound possesses estrogenic activity (Chen et al., 2002; Okuda et al., 2011; Sidorkiewicz et al., 2017), acute toxicity (Moreman et al., 2017; Qiu et al., 2018), neurotoxicity (Kim et al., 2015; Kinch et al., 2015), immunotoxicity (Ma et al., 2015; Zhao et al., 2017; Dong et al., 2018; Qiu et al., 2018), reproductive and developmental toxicity (Naderi et al., 2014; Mersha et al., 2015; Ullah et al., 2017). In addition, BPS is strongly associated with obesity and steatosis (Peyre et al., 2014; Liu et al., 2017a; Rezg et al., 2018). It is much worse that, compared to BPA, BPS has a longer half-life period and poorer bioavailability (Gayrard et al., 2019), which lead to its removal more difficult and more expensive (Choi and Lee, 2017).

With the ever-rising concern on this problem, various methods, such as chlorination (Gao et al., 2018), biodegradation (Wang et al., 2019b), photochemical degradation (Kovačič et al., 2019), manganese dioxide and ferrate oxidation (Li et al., 2018; Yang et al., 2019), have been applied to eliminate BPS. Nevertheless, the long consuming time, high cost and complex pretreatment etc. hinder the practical

application of the aforementioned methods. Furthermore, BPS in these systems may be transformed into multifarious intermediates with unpredictable toxicity although the complete removal can be also achieved. In this regard, a green, effective and environment-friendly technology is urgently needed.

As a prospective technique, advanced oxidation processes (AOPs) can generate multitudes of reactive free radicals to destruct the pollutants with a high mineralization degree (Duan et al., 2018). Last decades have witnessed the comprehensively studied progress of persulfate (PS), and it is well-documented that sulfate radicals (SR, $SO_4^{\bullet-}$, E^0 = 2.6 ~ 3.1 V) and hydroxyl radicals (•OH, E^0 = 1.9 ~ 2.8 V) can be formed after PS activation (Oh et al., 2016; Wacławek et al., 2017; Ike et al., 2018; Lee et al., 2020). Common activation approaches include heat (Pan et al., 2018b), ultraviolet irradiation (Izadifard et al., 2017; Pan et al., 2018b), ultrasound (Lu et al., 2019), base (Peng et al., 2017), transition metals (Monteagudo et al., 2015; Pan et al., 2018b), natural organic matter (NOM) (Lu et al., 2016), ozone (Izadifard et al., 2017), quinones (Fang et al., 2013), and electrochemical reactions (Farhat et al., 2015). For instance, Liu et al. (2019b) and Lu et al. (2019) correspondingly used Fe@C activated peroxymonosulfate (PMS) and ultrasound triggered PS to remove aqueous BPS, and the complete removal of BPS at micromole level was obtained in minutes, indicating the excellent performance of SR-AOPs. Nevertheless, only 5 or 7 byproducts were reported in these works. The specific transformation intermediates and overall pathways of BPS in SR-AOPs circumstance are still less studied. Besides, phenolic organic compounds tend to polymerize when treated by general chemical methods (Chen et al., 2019; Dar et al., 2019; Cao et al., 2020; Xiang et al., 2020). As a kind of bisphenol category, it is unknown whether BPS can couple into its corresponding dimers, trimers and other complex either.

Currently, the ongoing interests have been attracted on nanocarbon-based catalysts for heterogeneous PS activation (Pan et al., 2018a). Extensive researches have elucidated the excellent catalyzed PS ability of carbonaceous materials, such as graphene (GP) (Chen and Carroll, 2016), reduced graphene oxide (rGO) (Wang et al., 2019a) and carbon nanotubes (CNTs) (Pan et al., 2018a; Cheng et al., 2019), to eliminate persistent organic pollutants efficiently. Furthermore, heteroatoms (e.g. N) doping can significantly improve their catalytic ability. Unfortunately, little knowledge on BPS removed by nanocarbon-based material activated PS can be obtained, yet.

In such cases, we investigated the overall BPS transformation behavior (including the kinetics performance, intermediates and reaction pathways) by using (N-doped) carbonaceous materials and heat activated PS. The purposes of the present research are to 1) test the effects of catalyst dosage, solution pH, initial substrate concentration and water matrix on BPS abatement in catalyzed PS system; 2) identify the probable reaction products and deduce the possible oxidation pathways of BPS by combined the results of LC-TOF-MS analysis and transition state calculation; and 3) explore the underlying effect of reaction temperature on the distribution and abundance of the identified intermediates of BPS. This research can provide a useful technique to treat the waters and wastewaters containing BPS and its analogues, and enrich our knowledge on the transformation behavior, trend and fate of BPS.

2. Materials And Methods

2.1 Reagents and water matrices

Details of reagents and water matrices used in this study were given in Text. S1.

2.2 Preparation and characterization of nitrogen-doped nanocarbon based materials

The nitrogen-doped nanocarbon based materials were prepared by thermal decomposition method and the specific preparation was shown in Text. S2, as well as their relative characterization results and discussion.

2.3 Experimental procedure

A series of kinetics experiments of BPS were carried out in a 250 mL conical flask containing a certain amount of BPS and catalyst, at 25°C in a SHA-B thermostatic water bath shaker (Boyuan, China). After stirred 30 min, the above reaction system could reach adsorption-desorption equilibrium (see Fig. S4). By adding 0.8 mL 0.1 M PS, the catalytic reaction was initiated. At the selected time points, 1 mL of the reaction solution were sampled and quickly filtered through a 0.22 μm teflon filter into a HPLC vial pre-added with 50 μL of 0.2 M $Na_2S_2O_3$ as terminating agent.

No catalyst was added for the single PS oxidation at ambient temperature as control. Consequently, the sampled reaction solution could be directly analyzed using HPLC instrument. Other experimental procedures were as same as that with catalyst. In order to figure out the transformation discrepancy of BPS during PS oxidation with and without catalyst, we also carried out the tests of heat activated PS oxidation at 65 ℃. We conducted all experiments in triplicate, and maintained the initial pH to the desired value by adding 0.1 M NaOH and H_2SO_4

2.4 Analytical methods

The residual concentrations of BPS were quantified using a Hitachi high-performance liquid chromatography (HPLC) system (Hitachi, Japan) equipped with a Zorbax 300SB-C18 column (150×4.6 mm, 5 μm) and a 5420 UV-Vis detector. The HPLC parameters were set as: 3‰ formic acid aqueous solution and methanol (v/v = 45/55) used as mobile phase at a flow rate of 1 mL min^{-1}, an injection volume of 80 μL, and a detection wavelength of 298 nm.

Before LC-MS analysis, sample solutions were purified by solid phase extraction (SPE) equipment to remove salts and particles. Specific processes could be found elsewhere (Liu et al., 2019a). The possible reaction intermediates of BPS were detected by an X500R QTOF mass spectrometer system (AB Sciex Pte. Ltd., USA) equipped with a Thermo BDS Hypersil C18 column (2.1×100 mm, 2.4 mm, Thermo Fisher Scientific, USA). The detail setups of HPLC-MS/MS were listed in Supporting Information (SI), Text. S3. All data were analyzed by using the SCIEX OS 1.6 software (AB Sciex).

The EPR spectra were recorded by an E500-9.5/12 electron paramagnetic resonance spectrometer (Bruker, German), using DMPO as a spin-trapping reagent for $SO_4^{\bullet-}$ and •OH detection.

The residual concentration of PS anion was measured with a Persee UV-Vis spectrophotometer (Beijing, China) at 352 nm.

2.5 Transition state calculation

Transition state calculation for the reactions of $SO_4^{\bullet-}$ and • OH with BPS was implemented by using Gaussian 09 software with the basis set of m062x/lanl2dz. The fact that only one negative eigenvalue of the Hessian matrix and intrinsic reaction coordinate (IRC) analysis were used to further verify the structures of the transition states (TSs). The energies (*E*) of reactants, TSs and products could be acquired from their relative output files by searching the key word “HF”, and the reaction barrier was then calculated to infer the possible reaction pathways.

3. Results And Discussion

3.1 Removal of BPS by activated PS

3.1.1 Reaction kinetics of BPS in PS/(N-)SWCNTs system

Five nanocarbon-based materials especially SWCNTs, showed the good adsorption and activation PS potential to remove aqueous BPS and this performance could be promoted after N doping (Text. S4). Thus, SWCNTs and N-SWCNTs were chosen for subsequent research.

Figure 1 (a-c) revealed the effects of materials concentration, initial substrate concentration and solution pH on the removal of BPS in PS/N-SWCNTs system, respectively. As seen from Fig. 1 (a), the elimination rate of the substrate elevated with the increase of N-SWCNTs concentration, likely due to the increasing adsorption BPS capacity and more amounts of hydroxyl radicals in reaction solution (see Text. S5). Nevertheless, the increment in N-SWCNTs dosage were not positively related with BPS elimination rate. To be specific, the removal efficiency of BPS after the addition of 10 $mg{\cdot}L^{-1}$ N-SWCNTs was 63.8% in 90 min; then it suddenly ramped to 100.0% when the N-SWCNTs dosage was 20 $mg{\cdot}L^{-1}$. But just a bit elevation in BPS removal was found as it further reached 30 $mg{\cdot}L^{-1}$. This result was also observed in the reports of Liu et al. (2019b) and Cheng et al. (2017).

We also studied the effects of initial substrate concentrations (10, 20 and 30 μM) on BPS removal. From Fig. 1 (b), we could see that the removal rate of BPS decreased as its initial concentration increased. For a certain PS concentration, we considered a constant amount of active species generated in solution, which led to a high removal rate at a low initial BPS concentration. Besides, the higher concentration of target compound would result in the more formation of reaction intermediates, and their competition with BPS for oxidants and active sites upon N-SWCNTs inevitably inhibited the removal of the parent compound.

In Fig. 1 (c), there was no obvious effects on the removal trend of BPS at initial pH 5.0, 7.0 and 9.0. Additionally, the decrease adsorption of target compound at pH 5.0 might be attributed to the existence of surface oxygenic functional groups (e.g., −COOH and − OH) on SWCNTs as indicated by the measured O content in Table. S2. The restrained deprotonation of the acidic functional groups (− COOH and − OH) of SWCNTs at this pH further inhibited π-electron-donor ability of the graphene surface, which therefore resulted in weakening π − π electron-donor-acceptor interactions between aromatic compound and SWCNTs (Chen et al., 2008). In fact, the solution pH is a vital factor during persulfate oxidation process and the pH variation can largely change the removal rate of the substrates via impacting the species distribution and contribution of the generated reactive oxygen species (ROS), as well as the changing existing states of organic compounds (Qi et al., 2021). However, most of impacts could be overlaid or ignored possibly on account of the proliferated ROS content derived from the catalytic performance of nanocarbon-based materials towards persulfate (Pan et al., 2018a). This result suggested that the PS/nanocarbon-based catalysts technique can be applied in a large pH range.

Figure 1 (d) depicted the removal of BPS by PS activated with SWCNTs and N-SWCNTs under the optimal conditions: 1.0 mM PS, 20 mg·L^{-1} catalyst, initial pH 7.0 and 25 ℃. Obviously, 96.0% removal of 10 μM BPS could be obtained in 90 min reaction for the case of SWCNTs. Just as we discussed above, a promotion on both adsorption and activation after N doping was observed. This activation effect was highly consistent with the results of residual PS concentration (Fig. S5).

3.1.2 Degradation of BPS in different water matrices

Three different water samples, including Tap water, River water, and Secondary effluent were used to explore the application potential of N-SWCNTs/PS technique for the elimination of BPS. The reaction temperature was maintained at 25 ℃ and no pH adjustment was conducted. As seem from Fig. S6, the (nearly) complete removal of BPS in Ultrapure water and Tap water was obtained, while it declined to 80.3% and 52.3% for River water and Secondary effluent, respectively, due to the high TOC level shown in Table S4.

3.2 Intermediates identification and reaction pathways elucidation

The experiments for LC-MS analysis were carried out under the optimal kinetics conditions for PS-catalyst system. Given the possible effect of reaction temperature on BPS transformation, we also conducted the single PS activated by heat test for comparison. As shown in Fig. S8, heat activated PS could also degrade BPS effectively and thus we took 65 ℃ as an example. Based on our detailed analysis, overall, we identified a total of 15 intermediates in two regimes (12 for PS-catalyst and 14 for PS-heat system). Moreover, all the calculated errors between the measured mass values and the proposed theoretical molecular formulas were not more than 5 ppm (Table S5), demonstrating the high reliability of the structural assignments. The specific structures of these intermediates and inferred transformation pathways in PS/N-SWCNTs and PS-heat systems were summarized in Figs. 2, 3 and S11.

3.2.1 The PS/N-SWCNTs system

The *m/z* values ranged from 93.03 to 761.04 among 12 by-products (labeled as P1-P11 and P14) detected in the PS/N-SWCNTs system. For P1-P6, their *m/z* values were very close to that of BPS, while they were as 1.4–3.1 times as high as 249.02, implying that P1-P6, P9-P11 and P14 might be the analogues and coupling products of BPS, respectively. The highest peak area of all these 12 by-products obtained from LC-MS spectra were recorded in Fig. S9. Obviously, the peak area of P4, P6, P10 and P11 were much higher than others, indicating they were major intermediates of BPS. Therefore, their MS/MS spectra in detail were illustrated in Fig. 2 as examples. As seen, three daughter ions with *m/z* values of 155.99, 108.02 and 92.03 in the compound P4 were attributed to the stepwise losses of C_5H_5O (81 Da), SO (48 Da) and O (16 Da), respectively. Hence, P4 was recognized as a decarbonylation derivative of P3 (a secondary by-product of BPS), and its structure was displayed in Fig. 2. As for compound P6, the BPS fragment ion with *m/z* 249.02 was observed, which was resulted from the loss of carboxyl group (– COO) from the parent ion of *m/z* 293.01, indicating that P6 was a carboxylation product of BPS. The BPS fragment ion was also found in the MS/MS spectrum of compound P10 (*m/z* 405.01), which corresponded to the loss of sulfonylphenol fragment ion (156 Da). Therefore, P10 was identified as a cross-coupling product of the BPS substrate and sulfonylphenol P8. Similarly, P11 could be inferred as the dimer of BPS. The rest MS/MS spectra could be found in Fig. S11. Herein, there were four pairs of isomers, including hydroxylation product P1, and coupling products P9, P10 and P11.

Based on the identified intermediates, we proposed five transformation pathways of BPS in PS/N-SWCNTs solution, shown in Fig. 3. Pathway I was regarded as the hydroxylation of BPS, leading to the formation of P1 and P2. Meanwhile, P4 was generated by the decarbonylation of P3, an intermediate which came from the direct oxidation of P1. Potakis et al. (2016) also found PS treatment could make benzene ring of BPA opening. Pathway II and Pathway III were sulfate addition and carboxylation, respectively, and correspondingly produced sulfate addition product P5 and the carboxylation product P6. Recent studies on SR-AOPs have reported sulfate addition and carboxylation products, such as in the oxidation process of dimethyl phthalate (Xu et al., 2015), terbutaline (Zhou et al., 2017), nonylphenol triclosan (Qi et al., 2021), BPA (Sharma et al., 2016; Ding et al., 2020), diclofenac (Wu et al., 2019), and natrual organic matters (Jing et al., 2020). Given that these two kinds of addition products have been identified as intermediates for various substrates, sulfate addition and carboxylation should be the significant pathways during SR-AOPs and worth to be well considered.

As illustrated in Fig. 3, the cleavage of S – C bond was degradation pathway IV of BPS to further generate the phenol P7 and sulfonyl phenol P8. These two mono-benzene ring products resulted from BPS scission had been detected in various systems, such as ultrasound/PS (Lu et al., 2019), heat/PS (Wang et al., 2017), $CuCo_2S_4$/PMS (Haodan et al., 2018), and boron/PS (Shao et al., 2017), indicating that the cleavage of S – C bond was the common pathway during BPS oxidation.

After underwent H abstraction of hydroxyl radicals or electron transfer of sulfate radicals, BPS and its phenolic intermediates could self- and cross-couple into its oligomers (P9-P11, and P14) as Pathway V.

Thanks to the highest abundance of P10 and P11 shown in Fig. S9, polymerization reaction was mainly responsible for BPS transformation in this system. In general, the radical polymerization of organic compounds has two routes, namely, C – C and C – O coupling, thus resulting in two different structures of P9-P11 in this work. Surprisingly, we failed to detect the trimer of BPS in this system, but its hydroxylated product P14 with the *m/z* value of 761.05 appeared. The opposite data were obtained in PS-heat system (discussed below). Therefore, we deduced that P14 should be formed from the cross-coupling reaction of P1 and P11, while the self-coupling of BPS radicals yielded its relative trimer P15. Many studies have revealed that the coupling behaviors derive from the reaction of the corresponding radicals (Shao et al., 2017; Haodan et al., 2018; Chen et al., 2020; Yao et al., 2020). Our previous work even found a multitude of coupling products during the photodegradation of polyfluorinated dibenzo-*p*-dioxins (PFDDs) on silica gel (Qu et al., 2019). In these above researches, coupling reaction always plays a vital role on the transformation of all the selected compounds. Therefore, it warrants further deep study.

3.2.2 The PS-heat system

Main reaction intermediates and transformation pathways of BPS in PS-heat reaction solution were the same with those in PS/N-SWCNTs system. Specifically, eleven intermediates (P1-P11) occurred in these two systems. Although the reactive mechanisms of these two solutions were same (radical control), unique products were identified. For example, the hydroxylated trimers of BPS (P14) disappeared while the coupling products (P12, P13 and P15) were detected in PS-heat condition. Furthermore, their peak area were largely different with each other (Figs. S9 and S10). Generally, the peak area of these 14 products in PS-heat solution were relatively higher than those in PS-catalyst circumstance. Zrinyi et al. (2017) in 2017 systematically investigated the effect of reaction temperature on the transformation pathway of benzoic acid oxidized by PS and the results showed product distribution indeed differed with changed temperature. They also found that $SO_4^{\bullet-}$ mainly contributed to the transformation of substrate at 70 ℃ (very approximate to 65 ℃ used in this work), whereas, •OH was considered as the dominant active species under the PS activated by N-doping single wall carbon nanotubes. The dominant role of $SO_4^{\bullet-}$ might produce more radicals of BPS and its phenolic intermediates by electron transfer, and further lead to the more generation of polymers in the PS-heat. Another likelihood was attributed to the loss of some BPS by nanocarbon materials adsorption when sampled.

In summary, the observations showed that BPS would be subjected to hydroxylation, sulfate addition, carboxylation, the cleavage of S – C bond and polymerization during PS oxidation. However, the distribution and abundance of products differed depending on the dominant ROS.

3.3 Theoretical calculation

In general, three reaction mechanisms, namely radical adduct formation (RAF), hydrogen atom abstraction (HAA), and single electron transfer (SET) are deduced as three possible initial oxidation reactions of $SO_4^{\bullet-}$ and •OH with phenolic organic contaminants (POCs), suggested by previous reaserches (Neta et al., 1977; vonSonntag, 1996). The experimental and theoretical results demonstrate that $SO_4^{\bullet-}$ can oxidize POCs with electron-rich groups via SET mechanism (Minisci et al., 1983; Pan et al.,

2017; Mei et al., 2019). Figure 4 (a) depicted the specific SET mechanism of $SO_4^{\bullet-}$ with BPS. As shown, BPS was firstly transformed into a transient cationic intermediate by electron transfer of $SO_4^{\bullet-}$, and then BPS radical ($C_{12}H_9O_4S\bullet$) could be yielded rapidly after lost a proton. The combination of $C_{12}H_9O_4S\bullet$ with its resonance forms caused by the delocalization of the unpaired electron resulted in the formation of polymeric intermediates (Dec and Bollag, 1994; Chen et al., 2020). Meanwhile, the TSs between $SO_4^{\bullet-}$ and BPS were calculated to examine the possible sites of RAF occurrence (Fig. 4 (b)). Due to the interaction between $SO_4^{\bullet-}$ and the other hydroxyl group of BPS, we cannot accurately calculate reaction barriers of 3C and 5C. Therefore, the reaction barriers at C (2) and C (6) were shown in Fig. 4 (b). As seen, their ΔE values were quite low (13.85 kJ/mol for C (2) and 14.00 kJ/mol for C (6)), further confirming the specific structure of sulfate addition product P5.

For •OH, RAF and HAA are generally suggested to be the initial oxidation reactions. Therefore, considering the symmetry of BPS molecular structure, steric hindrance and electron donating group, four possible carbon sites (2C, 3C, 5C and 6C) and five possible hydrogen sites (1H, 2H, 3H, 4H and 5H) in total for •OH attack were calculated. The corresponding energy profiles were shown in Fig. 5. It was seen that the ΔE values at C (2), C (3), C (5) and C (6) sites were 22.20, 23.75, 24.07 and 26.95 kJ/mol, respectively, comparable to those shown in Fig. 4 (b). The reaction barriers at five hydrogen sites by HAA were much higher than those by RAF, except for ΔE at H (1); and their specific values were 25.06 (1), 70.93 (2), 64.20 (3 and 4) and 54.88 (5) kJ/mol. Consequently, RAF and HAA could easily occur at C (2), C (3), C (5), C (6) and H (1) places. However, only two peaks of hydroxylation product P1 were detected from total ion current (TIC) chromatograph, suggesting hydroxyl group preferred to link to C (2) and C (3) sites of BPS, just as depicted in Fig. 3. The generated $C_{12}H_9O_4S\bullet$ radical after •OH abstracted H could participate in the subsequent coupling reaction. The detection of hydroxyl addition and coupling products P1, P2 and P9 ~ P15 further verified this result.

4. Conclusion

N-SWCNTs and heat showed the good activation PS potential to remove aqueous BPS. Under the conditions of $[BPS]_0$: $[PS]_0$ = 1: 100, T = 25 ℃, pH_0 = 7.0, [N-SWCNTs] = 20 $mg{\cdot}L^{-1}$, 10 μM BPS could be completely removed in 90 min. The removal rate was improved with the increase in materials dosage at low initial concentration of BPS. TOC content was highly related with BPS elimination in real water matrices. According to LC-MS analysis, 12 products were generated in PS/N-SWCNTs system, and hydroxylation, sulfate addition, carboxylation, the cleavage of S − C bond and polymerization were responsible for their generation. Some unique products were found in PS-heat situation. The distribution and abundance of BPS intermediates differed depending on the dominant ROS involved. The calculated reaction barriers of hydroxylation, hydrogen atom and sulfate addition reaction based on transition state theory further verified the above proposed mechanisms.

Declarations

Ethics approval and consent to participate Not applicable

Consent for publication Not applicable

Availability of data and materials All data generated or analyzed during this study are included in this published article [and its supplementary information files].

Competing interests The authors declare that they have no competing interests

Funding This research was financially supported by the Major Science and Technology Program for Water Pollution Control and Treatment of China (No. 2018ZX07208001-06), the Fundamental Research Funds for the Central Universities (No. 14380137) and the National Natural Science Foundation of China (No. 22076076, 21876082).

Authors' contributions Junyan Wei: Investigation, Data curation, Writing - original draft, Software. Linning Yin: Data curation. Ruijuan Qu: Validation. Gadah Al-Basher: Validation. Xiaoxue Pan: Methodology, Writing - review & editing. Zunyao Wang: Writing - review & editing, Supervision.

Acknowledgements This research was financially supported by the Major Science and Technology Program for Water Pollution Control and Treatment of China (No. 2018ZX07208001-06), the Fundamental Research Funds for the Central Universities (No. 14380137) and the National Natural Science Foundation of China (No. 22076076, 21876082).

References

1. Cao K, Popovic Z, Smith, Dabeka (2019) LC-MS/MS analysis of bisphenol S and five other bisphenols in total diet food samples. Food Addit Contam Part A-Chem 36:1740–1747. https://doi.org/10.1080/19440049.2019.1643042
2. Cao W, Yu Y, Wei J, Al-Basher G, Pan X, Li B, Xu X, Alsultan N, Chen J, Qu R, Wang Z (2020) KMnO4-mediated reactions for hexachlorophene in aqueous solutions: Direct oxidation, self-coupling, and cross-coupling. Chemosphere 259:127422. https://doi.org/10.1016/j.chemosphere.2020.127422
3. Chen C, Wu Z, Zheng S, Wang L, Niu X, Fang J (2020) Comparative Study for Interactions of Sulfate Radical and Hydroxyl Radical with Phenol in the Presence of Nitrite. Environ Sci Technol 54:8455–8463. https://doi.org/10.1021/acs.est.0c02377
4. Chen H, Carroll KC (2016) Metal-free catalysis of persulfate activation and organic-pollutant degradation by nitrogen-doped graphene and aminated graphene. Environ Pollut 215:96–102. https://doi.org/10.1016/j.envpol.2016.04.088
5. Chen J, Chen W, Zhu D (2008) Adsorption of Nonionic Aromatic Compounds to Single-Walled Carbon Nanotubes: Effects of Aqueous Solution Chemistry. Environ Sci Technol 42:7225–7230. https://doi.org/10.1021/es801412j

6. Chen J, Qi Y, Pan X, Wu N, Zuo J, Li C, Qu R, Wang Z, Chen Z (2019) Mechanistic insights into the reactivity of Ferrate(VI) with phenolic compounds and the formation of coupling products. Water Res 158:338–349. https://doi.org/10.1016/j.watres.2019.04.045
7. Chen MY, Ike M, Fujita M (2002) Acute toxicity, mutagenicity, and estrogenicity of bisphenol-A and other bisphenols. Environ Toxicol 17:80–86. https://doi.org/10.1002/tox.10035
8. Cheng X, Guo H, Zhang Y, Korshin GV, Yang B (2019) Insights into the mechanism of nonradical reactions of persulfate activated by carbon nanotubes: Activation performance and structure-function relationship. Water Res 157:406–414. https://doi.org/10.1016/j.watres.2019.03.096
9. Cheng X, Guo H, Zhang Y, Wu X, Liu Y (2017) Non-photochemical production of singlet oxygen via activation of persulfate by carbon nanotubes. Water Res 113:80–88. https://doi.org/10.1016/j.watres.2017.02.016
10. Choi YJ, Lee LS (2017) Aerobic soil biodegradation of bisphenol (BPA) alternatives bisphenol S and bisphenol AF compared to BPA. Environ Sci Technol 51:13698–13704. https://doi.org/10.1021/acs.est.7b03889
11. Dar AA, Wang X, Wang S, Ge J, Shad A, Ai F, Wang Z (2019) Ozonation of pentabromophenol in aqueous basic medium: Kinetics, pathways, mechanism, dimerization and toxicity assessment. Chemosphere 220:546–555. https://doi.org/10.1016/j.chemosphere.2018.12.154
12. Dec J, Bollag JM (1994) Dehalogenation of Chlorinated Phenols during Oxidative Coupling. Environ Sci Technol 28:484–490. https://doi.org/10.1021/es00052a022
13. Ding J, Bu L, Zhao Q, Kabutey FT, Wei L, Dionysiou DD (2020) Electrochemical activation of persulfate on BDD and DSA anodes: Electrolyte influence, kinetics and mechanisms in the degradation of bisphenol A. J Hazard Mater 388: 121789. https://doi.org/10.1016/j.jhazmat.2019.121789
14. Dong X, Zhang Z, Meng S, Pan C, Yang M, Wu X, Yang L, Xu H (2018) Parental exposure to bisphenol A and its analogs influences zebrafish offspring immunity. Sci Total Environ 610–611:291–297. https://doi.org/10.1016/j.scitotenv.2017.08.057
15. Duan X, Sun H, Shao Z, Wang S (2018) Nonradical reactions in environmental remediation processes: uncertainty and challenges. Appl Catal B-Environ 224:973–982. https://doi.org/10.1016/j.apcatb.2017.11.051
16. Fang G, Gao J, Dionysiou DD, Liu C, Zhou D (2013) Activation of persulfate by quinones: free radical reactions and implication for the degradation of PCBs. Environ Sci Technol 47:4605–4611. https://doi.org/10.1021/es400262n
17. Farhat A, Keller J, Tait S, Radjenovic J (2015) Removal of persistent organic contaminants by electrochemically activated sulfate. Environ Sci Technol 49:14326–14333. https://doi.org/10.1021/acs.est.5b02705
18. Gao Y, Jiang J, Zhou Y, Pang S-Y, Ma J, Jiang C, Yang Y, Huang Z-s, Gu J, Guo Q (2018) Chlorination of bisphenol S: Kinetics, products, and effect of humic acid. Water Res 131:208–217. https://doi.org/10.1016/j.watres.2017.12.049

19. Gayrard V, Lacroix MZ, Grandin FC, Collet SH, Picard-Hagen N (2019) Oral Systemic Bioavailability of Bisphenol A and Bisphenol S in Pigs. Environ Health Perspect 127:077005. https://doi.org/10.1289/EHP4599
20. Haodan X, Da W, Jun M, Tao Z, Xiaohui L, Zhiqiang C (2018) A superior active and stable spinel sulfide for catalytic peroxymonosulfate oxidation of bisphenol S. Appl Catal B-Environ 238:557–567. https://doi.org/10.1016/j.apcatb.2018.07.058
21. Ike IA, Linden KG, Orbell JD, Duke M (2018) Critical review of the science and sustainability of persulphate advanced oxidation processes. Chem Eng J 338:651–669. https://doi.org/10.1016/j.cej.2018.01.034
22. Izadifard M, Achari G, Langford CH (2017) Degradation of sulfolane using activated persulfate with UV and UV-Ozone. Water Res 125:325–331. https://doi.org/10.1016/j.watres.2017.07.042
23. Jin H, Zhu L (2016) Occurrence and partitioning of bisphenol analogues in water and sediment from Liaohe River Basin and Taihu Lake, China. Water Res 103:343–351. https://doi.org/10.1016/j.watres.2016.07.059
24. Jing K, Kong D, Lu J (2020) Change of disinfection byproducts formation potential of natural organic matter after exposure to persulphate and bicarbonate. Water Res 182:115970. https://doi.org/10.1016/j.watres.2020.115970
25. Kim B, Colon E, Chawla S, Vandenberg LN, Suvorov A (2015) Endocrine disruptors alter social behaviors and indirectly influence social hierarchies via changes in body weight. Environ Health 14:64. https://doi.org/10.1186/s12940-015-0051-6
26. Kinch CD, Ibhazehiebo K, Jeong JH, Habibi HR, Kurrasch DM (2015) Low-dose exposure to bisphenol A and replacement bisphenol S induces precocious hypothalamic neurogenesis in embryonic zebrafish. Proc. Natl. Acad. Sci. U. S. A. 112: 1475–1480. https://doi.org/10.1073/pnas.1417731112
27. Kovačič A, Gys C, Kosjek T, Covaci A, Heath E (2019) Photochemical degradation of BPF, BPS and BPZ in aqueous solution: Identification of transformation products and degradation kinetics. Sci Total Environ 664:595–604. https://doi.org/10.1016/j.scitotenv.2019.02.064
28. Lee J, von Gunten U, Kim J-H (2020) Persulfate-Based Advanced Oxidation: Critical Assessment of Opportunities and Roadblocks. Environ Sci Technol 54:3064–3081. https://doi.org/10.1021/acs.est.9b07082
29. Lehmler H-J, Liu B, Gadogbe M, Bao W, (2018) Exposure to Bisphenol A, Bisphenol F, Bisphenol S in U.S. Adults and Children: The National Health and Nutrition Examination Survey 2013–2014. ACS Omega 3: 6523–6532. https://doi.org/10.1021/acsomega.8b00824
30. Li J, Pang SY, Zhou Y, Sun S, Wang L, Wang Z, Gao Y, Yang Y, Jiang J (2018) Transformation of bisphenol AF and bisphenol S by manganese dioxide and effect of iodide. Water Res 143:47–55. https://doi.org/10.1016/j.watres.2018.06.029
31. Liao C, Kannan K (2014a) A Survey of Alkylphenols, Bisphenols, and Triclosan in Personal Care Products from China and the United States. Arch Environ Contam Toxicol 67:50–59. https://doi.org/10.1007/s00244-014-0016-8

32. Liao C, Kannan K (2014b) A survey of bisphenol A and other bisphenol analogues in foodstuffs from nine cities in China. Food Addit Contam Part A-Chem 31:319–329. https://doi.org/10.1080/19440049.2013.868611
33. Liao C, Liu F, Alomirah H, Loi VD, Mohd MA, Moon H-B, Nakata H, Kannan K (2012a) Bisphenol S in Urine from the United States and Seven Asian Countries: Occurrence and Human Exposures. Environ Sci Technol 46:6860–6866. https://doi.org/10.1021/es301334j
34. Liao C, Liu F, Kannan K (2012b) Bisphenol S, a new bisphenol analogue, in paper products and currency bills and its association with bisphenol A residues. Environ Sci Technol 46:6515–6522. https://doi.org/10.1021/es300876n
35. Liu B, Lehmler H-J, Sun Y, Xu G, Liu Y, Zong G, Sun Q, Hu FB, Wallace RB, Bao W (2017a) Bisphenol A substitutes and obesity in US adults: analysis of a population-based, cross-sectional study. Lancet Planet Health 1:e114–e122. https://doi.org/10.1016/S2542-5196(17)30049-9
36. Liu H, Yao J, Wang L, Wang X, Qu R, Wang Z (2019a) Effective degradation of fenitrothion by zero-valent iron powder (Fe0) activated persulfate in aqueous solution: Kinetic study and product identification. Chem Eng J 358:1479–1488. https://doi.org/10.1016/j.cej.2018.10.153
37. Liu Y, Guo H, Zhang Y, Cheng X, Zhou P, Wang J, Li W (2019b) Fe@C carbonized resin for peroxymonosulfate activation and bisphenol S degradation. Environ Pollut 252:1042–1050. https://doi.org/10.1016/j.envpol.2019.05.157
38. Liu Y, Zhang S, Song N, Guo R, Chen M, Mai D, Yan Z, Han Z, Chen J (2017b) Occurrence, distribution and sources of bisphenol analogues in a shallow Chinese freshwater lake (Taihu Lake): Implications for ecological and human health risk. Sci Total Environ 599–600: 1090–1098. https://doi.org/10.1016/j.scitotenv.2017.05.069
39. Lu J, Dong W, Ji Y, Kong D, Huang Q (2016) Natural organic matter exposed to sulfate radicals increases its potential to form halogenated disinfection byproducts. Environ Sci Technol 50:5060–5067. https://doi.org/10.1021/acs.est.6b00327
40. Lu X, Zhao J, Wang Q, Wang D, Xu H, Ma J, Qiu W, Hu T (2019) Sonolytic degradation of bisphenol S: Effect of dissolved oxygen and peroxydisulfate, oxidation products and acute toxicity. Water Res 165:114969. https://doi.org/10.1016/j.watres.2019.114969
41. Ma M, Crump D, Farmahin R, Kennedy SW (2015) Comparing the effects of tetrabromobisphenol-A, bisphenol A, and their potential replacement alternatives, TBBPA-bis(2,3-dibromopropyl ether) and bisphenol S, on cell viability and messenger ribonucleic acid expression in chicken embryonic hepatocytes. Environ Toxicol Chem 34:391–401. https://doi.org/10.1002/etc.2814
42. Mei Q, Sun J, Han D, Wei B, An Z, Wang X, Xie J, Zhan J, He M (2019) Sulfate and hydroxyl radicals-initiated degradation reaction on phenolic contaminants in the aqueous phase: Mechanisms, kinetics and toxicity assessment. Chem Eng J 373:668–676. https://doi.org/10.1016/j.cej.2019.05.095
43. Mersha MD, Patel BM, Patel D, Richardson BN, Dhillon HS (2015) Effects of BPA and BPS exposure limited to early embryogenesis persist to impair non-associative learning in adults. Behav Brain Funct 11:27. https://doi.org/10.1186/s12993-015-0071-y

44. Minisci F, Citterio A, Giordano C (1983) Electron-transfer processes: peroxydisulfate, a useful and versatile reagent in organic chemistry. Accounts Chem Res 16:27–32. https://doi.org/10.1002/chin.198326358
45. Monteagudo J, Durán A, González R, Expósito A (2015) In situ chemical oxidation of carbamazepine solutions using persulfate simultaneously activated by heat energy, UV light, Fe2 + ions, and H2O2. Appl Catal B-Environ 176:120–129. https://doi.org/10.1016/j.apcatb.2015.03.055
46. Moreman J, Lee O, Trznadel M, David A, Kudoh T, Tyler CR (2017) Acute Toxicity, Teratogenic, and Estrogenic Effects of Bisphenol A and Its Alternative Replacements Bisphenol S, Bisphenol F, and Bisphenol AF in Zebrafish Embryo-Larvae. Environ Sci Technol 51:12796–12805. https://doi.org/10.1021/acs.est.7b03283
47. Naderi M, Wong MYL, Gholami F (2014) Developmental exposure of zebrafish (Danio rerio) to bisphenol-S impairs subsequent reproduction potential and hormonal balance in adults. Aquat Toxicol 148:195–203. https://doi.org/10.1016/j.aquatox.2014.01.009
48. Neta P, Madhavan V, Zemel H, Fessenden RW (1977) Rate constants and mechanism of reaction of sulfate radical anion with aromatic compounds. J Am Chem Soc 99:163–164. https://doi.org/10.1016/S2542-5196(17)30049-9
49. Oh WD, Dong Z, Lim TT (2016) Generation of sulfate radical through heterogeneous catalysis for organic contaminants removal: Current development, challenges and prospects. Appl Catal B-Environ 194:169–201. https://doi.org/10.1016/j.apcatb.2016.04.003
50. Okuda K, Fukuuchi T, Takiguchi M, Yoshihara Si (2011) Novel pathway of metabolic activation of bisphenol A-related compounds for estrogenic activity. Drug Metab Dispos 39:1696–1703. https://doi.org/10.1124/dmd.111.040121
51. Pan X, Chen J, Wu N, Qi Y, Xu X, Ge J, Wang X, Li C, Qu R, Sharma VK (2018a) Degradation of aqueous 2, 4, 4'-Trihydroxybenzophenone by persulfate activated with nitrogen doped carbonaceous materials and the formation of dimer products. Water Res 143:176–187. https://doi.org/10.1016/j.watres.2018.06.038
52. Pan X, Yan L, Li C, Qu R, Wang Z (2017) Degradation of UV-filter benzophenone-3 in aqueous solution using persulfate catalyzed by cobalt ferrite. Chem Eng J 326:1197–1209. https://doi.org/10.1016/j.cej.2017.06.068
53. Pan X, Yan L, Qu R, Wang Z (2018b) Degradation of the UV-filter benzophenone-3 in aqueous solution using persulfate activated by heat, metal ions and light. Chemosphere 196:95–104. https://doi.org/10.1016/j.chemosphere.2017.12.152
54. Peng H, Xu L, Zhang W, Liu F, Lu X, Lu W, Danish M, Lin K (2017) Different kinds of persulfate activation with base for the oxidation and mechanism of BDE209 in a spiked soil system. Sci Total Environ 574:307–313. https://doi.org/10.1016/j.scitotenv.2016.09.057
55. Peyre L, Rouimi P, de Sousa G, Héliès-Toussaint C, Carré B, Barcellini S, Chagnon M-C, Rahmani R (2014) Comparative study of bisphenol A and its analogue bisphenol S on human hepatic cells: A

focus on their potential involvement in nonalcoholic fatty liver disease. Food Chem Toxicol 70:9–18. https://doi.org/10.1016/j.fct.2014.04.011

56. Potakis N, Frontistis Z, Antonopoulou M, Konstantinou I, Mantzavinos D (2016) Oxidation of bisphenol A in water by heat-activated persulfate. J Environ Manage 195:125–132. https://doi.org/10.1016/j.jenvman.2016.05.045
57. Qi Y, Wei J, Qu R, Al-Basher G, Pan X, Dar AA, Shad A, Zhou D, Wang Z (2021) Mixed oxidation of aqueous nonylphenol and triclosan by thermally activated persulfate: Reaction kinetics and formation of co-oligomerization products. Chem Eng J 403:126396. https://doi.org/10.1016/j.cej.2020.126396
58. Qiu W, Shao H, Lei P, Zheng C, Qiu C, Yang M, Zheng Y (2018) Immunotoxicity of bisphenol S and F are similar to that of bisphenol A during zebrafish early development. Chemosphere 194:1–8. https://doi.org/10.1016/j.chemosphere.2017.11.125
59. Qu R, Pan X, Li C, Liu J, Wang X, Zeng X, Wang Z (2019) Formation of hydroxylated derivatives and coupling products from the photochemical transformation of polyfluorinated dibenzo-p-dioxins (PFDDs) on silica surfaces. Chemosphere 231:72–81. https://doi.org/10.1016/j.chemosphere.2019.05.074
60. Rezg R, Abot A, Mornagui B, Aydi S, Knauf C (2018) Effects of Bisphenol S on hypothalamic neuropeptides regulating feeding behavior and apelin/APJ system in mice. Ecotox Environ Safe 161:459–466. https://doi.org/10.1016/j.ecoenv.2018.06.001
61. Shao P, Duan X, Xu J, Tian J, Shi W, Gao S, Xu M, Cui F, Wang S (2017) Heterogeneous activation of peroxymonosulfate by amorphous boron for degradation of bisphenol S. J Hazard Mater 322:532–539. https://doi.org/10.1016/j.jhazmat.2016.10.020
62. Sharma J, Mishra IM, Kumar V (2016) Mechanistic study of photo-oxidation of Bisphenol-A (BPA) with hydrogen peroxide (H2O2) and sodium persulfate (SPS). J Environ Manage 166:12–22. https://doi.org/10.1016/j.jenvman.2015.09.043
63. Sidorkiewicz I, Zaręba K, Wołczyński Sa, Czerniecki J (2017) Endocrine-disrupting chemicals-Mechanisms of action on male reproductive system. Toxicol Ind Health 33:601–609. https://doi.org/10.1177/0748233717695160
64. Ullah H, Ambreen A, Ahsan N, Jahan S (2017) Bisphenol S induces oxidative stress and DNA damage in rat spermatozoa in vitro and disrupts daily sperm production in vivo. Toxicol Environ Chem 99:953–965. https://doi.org/10.1080/02772248.2016.1269333
65. VonSonntag C (1996) Degradation of aromatics by Advanced Oxidation Processes in water remediation: Some basic considerations. J Water Supply Res Technol-Aqua 45:84–91
66. Wacławek S, Lutze HV, Grübel K, Padil VVT, Černík M, Dionysiou DD (2017) Chemistry of persulfates in water and wastewater treatment: A review. Chem Eng J 330:44–62. https://doi.org/10.1016/j.cej.2017.07.132
67. Wang Q, Li L, Luo L, Yang Y, Yang Z, Li H, Zhou Y (2019a) Activation of persulfate with dual-doped reduced graphene oxide for degradation of alkylphenols. Chem Eng J 376:120891.

https://doi.org/10.1016/j.cej.2019.01.170

68. Wang Q, Lu X, Cao Y, Ma J, Jiang J, Bai X, Hu T (2017) Degradation of Bisphenol S by heat activated persulfate: kinetics study, transformation pathways and influences of co-existing chemicals. Chem Eng J 328:236–245. https://doi.org/10.1016/j.cej.2017.07.041
69. Wang W, Abualnaja KO, Asimakopoulos AG, Covaci A, Gevao B, Johnson-Restrepo B, Kumosani TA, Malarvannan G, Minh TB, Moon H-B, Nakata H, Sinha RK, Kannan K (2015) A comparative assessment of human exposure to tetrabromobisphenol A and eight bisphenols including bisphenol A via indoor dust ingestion in twelve countries. Environ Int 83:183–191. https://doi.org/10.1016/j.envint.2015.06.015
70. Wang X, Chen J, Ji R, Liu Y, Su Y, Guo R (2019b) Degradation of Bisphenol S by a Bacterial Consortium Enriched from River Sediments. Bull Environ Contam Toxicol 103:630–635. https://doi.org/10.1007/s00128-019-02699-7
71. Wu M, Fu K, Deng H, Shi J (2019) Cobalt tetracarboxyl phthalocyanine-manganese octahedral molecular sieve (OMS-2) as a heterogeneous catalyst of peroxymonosulfate for degradation of diclofenac. Chemosphere 219:756–765. https://doi.org/10.1016/j.chemosphere.2018.12.030
72. Xiang W, Qu R, Wang X, Wang Z, Bin-Jumah M, Allam AA, Zhu F, Huo Z (2020) Removal of 4-chlorophenol, bisphenol A and nonylphenol mixtures by aqueous chlorination and formation of coupling products. Chem Eng J 402:126140. https://doi.org/10.1016/j.cej.2020.126140
73. Xu LJ, Chu W, Gan L (2015) Environmental application of graphene-based CoFe2O4 as an activator of peroxymonosulfate for the degradation of a plasticizer. Chem Eng J 263:435–443. https://doi.org/10.1016/j.cej.2014.11.065
74. Yamazaki E, Yamashita N, Taniyasu S, Lam J, Lam PKS, Moon H-B, Jeong Y, Kannan P, Achyuthan H, Munuswamy N, Kannan K (2015) Bisphenol A and other bisphenol analogues including BPS and BPF in surface water samples from Japan, China, Korea and India. Ecotox Environ Safe 122:565–572. https://doi.org/10.1016/j.ecoenv.2015.09.029
75. Yang T, Wang L, Liu Y, Huang Z, He H, Wang X, Jiang J, Gao D, Ma J (2019) Comparative study on ferrate oxidation of BPS and BPAF: Kinetics, reaction mechanism, and the improvement on their biodegradability. Water Res 148:115–125. https://doi.org/10.1016/j.watres.2018.10.018
76. Yao J, Qu R, Wang X, Sharma VK, Shad A, Dar AA, Wang Z (2020) Visible light and fulvic acid assisted generation of Mn(III) to oxidize bisphenol A: The effect of tetrabromobisphenol A. Water Res 169:115273. https://doi.org/10.1016/j.watres.2019.115273
77. Ye X, Wong L-Y, Kramer J, Zhou X, Jia T, Calafat AM (2015) Urinary Concentrations of Bisphenol A and Three Other Bisphenols in Convenience Samples of U.S. Adults during 2000–2014. Environ Sci Technol 49:11834–11839. https://doi.org/10.1021/acs.est.5b02135
78. Zhao C, Tang Z, Yan J, Fang J, Wang H, Cai Z (2017) Bisphenol S exposure modulate macrophage phenotype as defined by cytokines profiling, global metabolomics and lipidomics analysis. Sci Total Environ 592:357–365. https://doi.org/10.1016/j.scitotenv.2017.03.035

79. Zhou J, Chen XH, Pan SD, Wang JL, Zheng YB, Xu JJ, Zhan YG, Cai ZX, Jin MC (2019) Contamination status of bisphenol A and its analogues (bisphenol S, F and B) in foodstuffs and the implications for dietary exposure on adult residents in Zhejiang Province. Food Chem 294:160–170. https://doi.org/10.1016/j.foodchem.2019.05.022
80. Zhou L, Sleiman M, Ferronato C, Chovelon J-M, de Sainte-Claire P, Richard C (2017) Sulfate radical induced degradation of β2-adrenoceptor agonists salbutamol and terbutaline: Phenoxyl radical dependent mechanisms. Water Res 123:715–723. https://doi.org/10.1016/j.watres.2017.07.025
81. Zrinyi N, Pham LT (2017) Oxidation of benzoic acid by heat-activated persulfate: Effect of temperature on transformation pathway and product distribution. Water Res 120:43. https://doi.org/10.1016/j.watres.2017.04.066

Figures

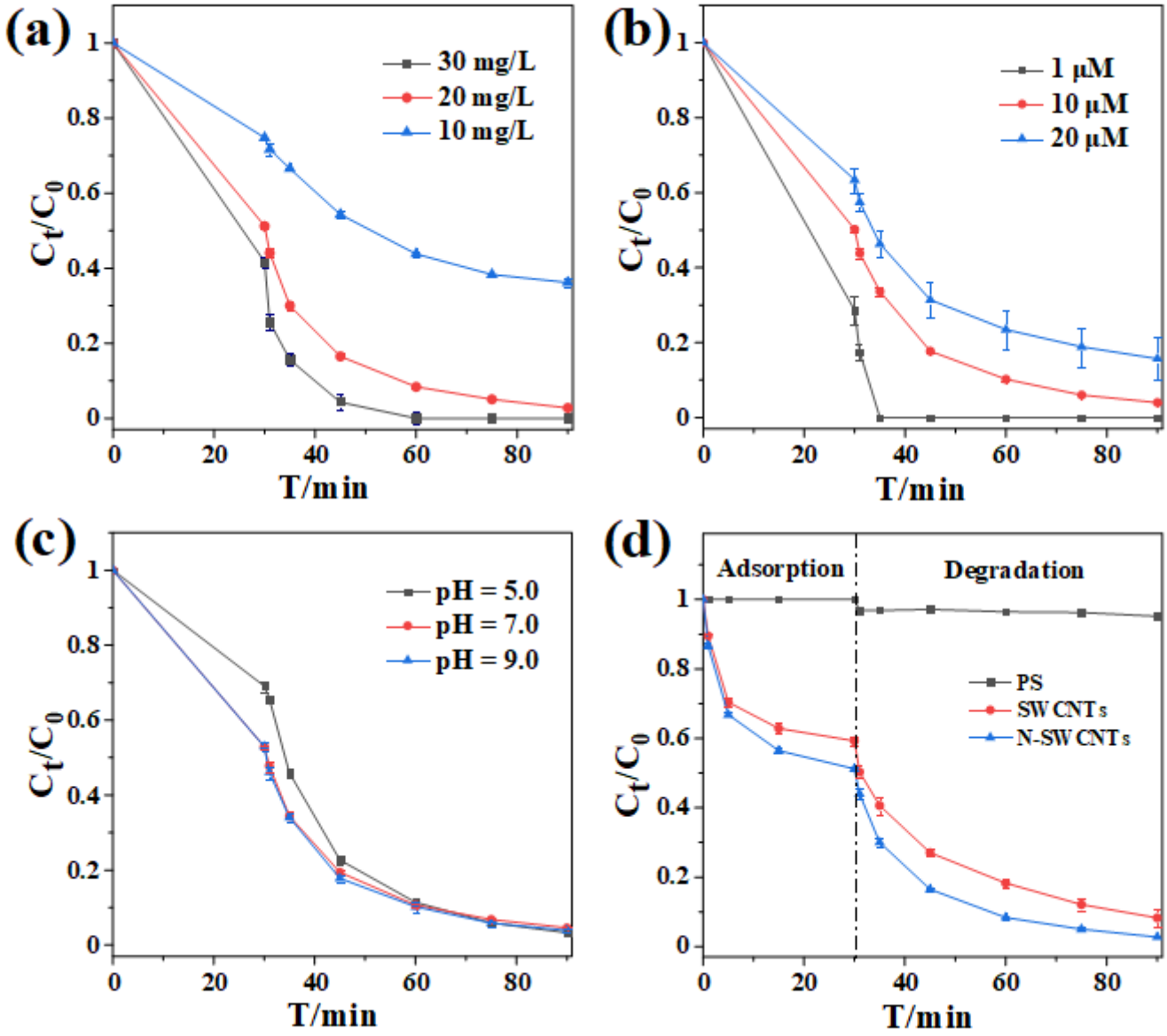

Figure 1

The effects of materials concentration (a), initial substrate concentration (b), solution pH (c); and N doping (d) on the degradation of BPS in PS/N-SWCNTs system. Conditions: [BPS]0 = 10 μM, [PS]0 = 1.0 mM, T = 25 °C, pH0 = 7.0, [(N-)SWCNTs] = 20 mg·L-1

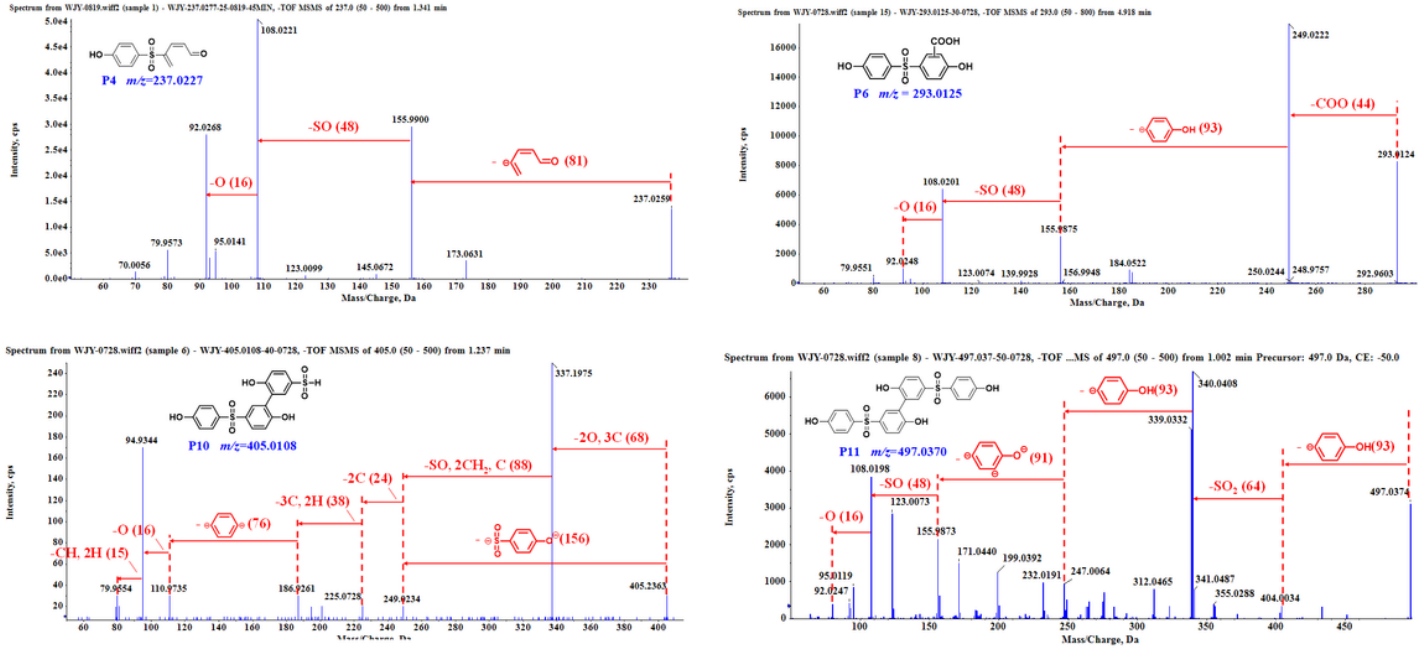

Figure 2

The MS/MS spectra of main products (P4, P6, P10 and P11) in the PS/N-SWCNTs system

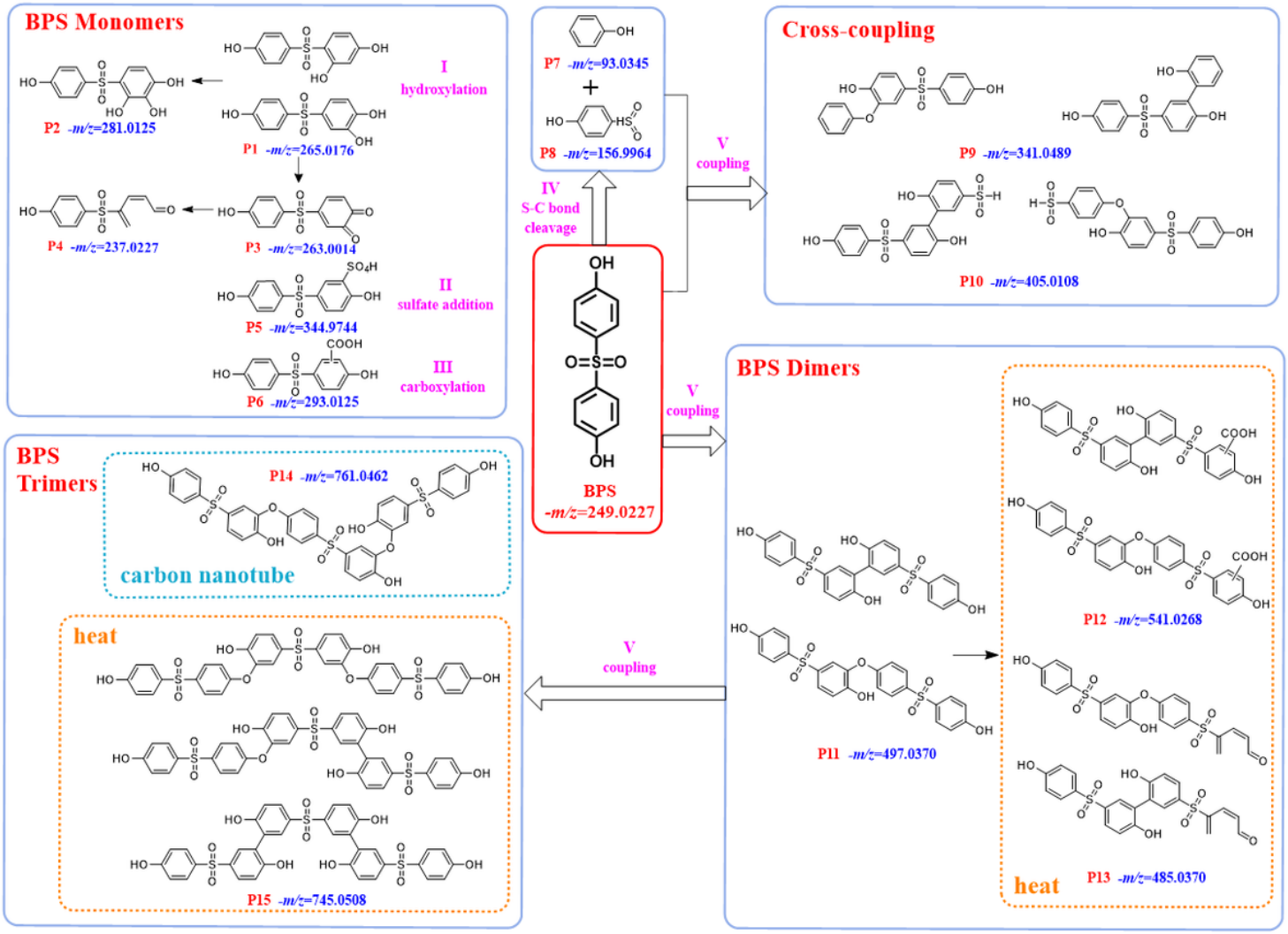

Figure 3

Transformation pathways of BPS in the PS/N-SWCNTs system and PS-heat system. Conditions: [BPS]0 = 10 μM, [PS]0 = 1.0 mM, pH0 = 7.0. Note that the intermediates not specified in this figure were common products in the two systems

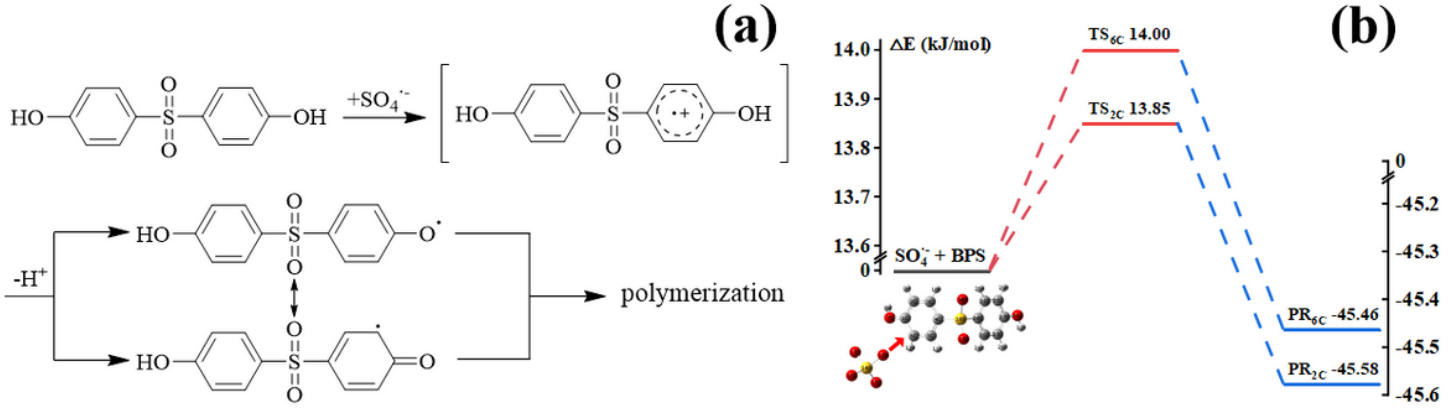

Figure 4

Scheme for the SET mechanism (a) and energy profiles (△E, kJ/mol) calculated at the m062x/lanl2dz level for the RAF mechanism (b) of SO4•− with BPS

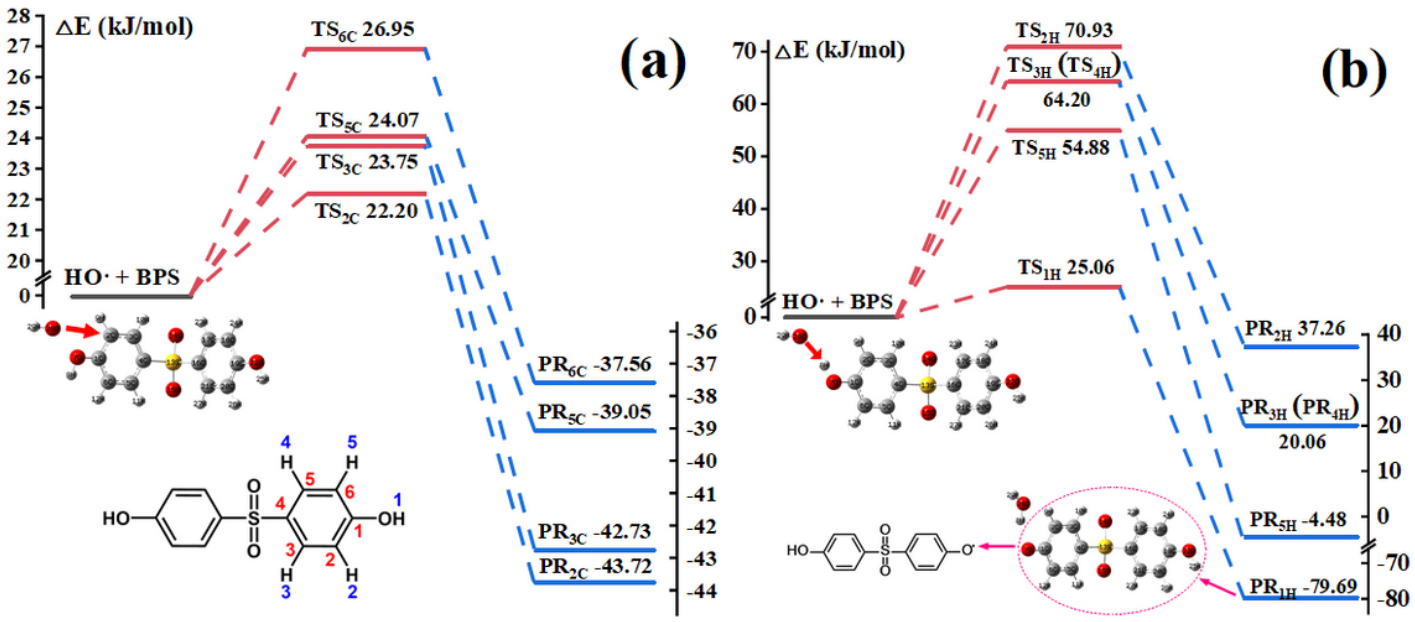

Figure 5

Energy profiles (△E, kJ/mol) calculated at the m062x/lanl2dz level for the RAF (a) and HAA (b) mechanisms of •OH with BPS

Supplementary Files

This is a list of supplementary files associated with this preprint. Click to download.

- SupportingInformation.docx